Supporting Information

Ambient Electrocatalytic Nitrogen Reduction on MoO_2/Graphene Hybrid: Experimental and DFT studies

Jing Wang[1#], Ya-ping Liu[1#], Hu Zhang[2], Da-jian Huang[1], Ke Chu [1*]

[1] *School of Materials Science and Engineering, Lanzhou Jiaotong University, Lanzhou 730070, China*

[2] *School of Materials Science and Engineering, University of Science and Technology Beijing, Beijing, 100083, China*

*Corresponding author. E-mail address: chukelut@163.com (K. Chu)

[#] These authors contributed equally to this work.

Experimental section

Synthesis of MoO_2/RGO

All the chemicals were used as received without further purification. The MoO_2/RGO was synthesized by a microwave-assisted hydrothermal approach based on a reported method with a slight modification[1]. Briefly, 50 ml of homogeneous GO suspension (1 mg mL^{-1}) was fabricated by dispersion of GO powder in distilled water under ultrasonication for 1 h. Then, 0.4 g of ammonium molybdate tetrahydrate and 0.04 g of ascorbic acid were sequentially added into GO suspension under vigorous stirring for 10 min. After that, the mixture was sealed and treated by a household microwave oven (2450 MHz) for 10 min. After cooling to room temperature, the precipitates were collected and washed several times with distilled water and then dried at 60°C for 12 h. Finally, the obtained powder was annealed at 400 °C for 2 h under Ar atmosphere. For comparison, the MoO_2 NPs and RGO alone were synthesized by the same procedure without addition of GO and ammonium molybdate tetrahydrate, respectively.

Electrochemical NRR measurements

Electrochemical measurements were performed on a CHI-660E electrochemical workstation using a standard three-electrode system, including Ag/AgCl electrode as the reference electrode, graphite rod as the counter electrode and catalyst loaded on carbon cloth (CC) as the working electrode. The working electrode was prepared by loading 0.2 mg cm^{-2} of catalyst onto the CC (1×1 cm^2). All potentials were referenced to a reversible hydrogen electrode (RHE) by $E_{\mathrm{RHE}} = E_{\mathrm{Ag/AgCl}} + 0.197 + 0.059 \times \mathrm{pH}$. The RHE calibration was experimentally conducted in the high-purity hydrogen saturated 0.1 M Na_2SO_4 electrolyte by cyclic voltammetry curves, with using graphite rod and Pt wire were used as the counter and working electrodes, respectively (Fig. S1). Prior to electrolysis, the cathodic compartment was purged with Ar for 30 min. During the electrolysis, N_2 gas (99.999% purity) was continuously fed into the cathodic compartment at a flow rate of 10 mL min^{-1}, and the electrolyte in the cathodic compartment was subjected to magnetic stirring at a rate of 300 rpm throughout the measurement. After electrolysis, the NH_3 yield and FE were determined by an indophenol blue method[2], and the possible N_2H_4 was determined by a method of Watt and Chrisp[3].

Determination of NH_3

The concentration of produced NH_3 in 0.1 M Na_2SO_4 was quantitatively determined by an indophenol blue method[4]. Typically, 4 mL of electrolyte was removed from the electrochemical reaction vessel. Then 50 μL of solution containing NaOH (0.75 M) and NaClO (ρ_{Cl} = ~4), 500 μL of solution containing 0.32 M NaOH, 0.4 M $C_7H_6O_3$, and 50 μL of $C_5FeN_6Na_2O$ solution (1 wt%) were sequentially added into the electrolyte. After standing for 2 h, the UV-Vis absorption spectrum was measured and the concentration-absorbance curves were calibrated by the standard NH_4Cl solution with a serious of concentrations (Fig. S2a).

Determination of N_2H_4

The N_2H_4 concentration was quantitatively determined by a method of Watt and Chrisp[3, 4]. Typically, 5 mL of electrolyte was removed from the electrochemical reaction vessel. The 330 mL of color reagent containing 300 mL of ethyl alcohol, 5.99 g of $C_9H_{11}NO$ and 30 mL of HCl were prepared, and 5 mL of color reagent was added into the electrolyte. After stirring for 10 min, the UV-Vis absorption spectrum was measured and the concentration-absorbance curves were calibrated by the standard N_2H_4 solution with a serious of concentrations (Fig. S3a).

Calculations of NH_3 yield and Faradaic efficiency

NH_3 yield was calculated by the following equation:

$$\mathrm{NH_3\ yield}\ (\mu\mathrm{g\ h^{-1}\ mg_{cat.}^{-1}}) = \frac{c_{\mathrm{NH_3}} \times V}{t \times m} \tag{1}$$

Faradaic efficiency was calculated by the following equation:

$$\text{Faradaic efficiency (\%)} = \frac{3 \times F \times c_{\mathrm{NH_3}} \times V}{17 \times Q} \times 100\% \tag{2}$$

where c_{NH3} is the measured NH_3 concentration, V is the volume of the electrolyte, t is the reduction time and m is the mass loading of catalyst on carbon paper. F is the Faraday constant, Q is the quantity of applied electricity.

Characterizations

Scanning electron microscopy (SEM) was performed on a JSM-6701 microscope. Transmission electron microscopy (TEM) and high-resolution transmission electron microscopy (HRTEM) were carried out on a Tecnai G^2 F20 microscope. X-ray diffraction (XRD) pattern was recorded on a Shimadzu 7000LX diffractometer. X-ray photoelectron spectroscopy (XPS) analysis was conducted on a PHI 5702 spectrometer. Temperature-programmed desorption (TPD) profiles were recorded on a Chem-BET 3000 (Quantachrome) apparatus. ^{1}H (NMR) spectra were collected on a 500 MHz Bruker superconducting-magnet NMR spectrometer.

Calculation details

DFT calculations were conducted using the CASTEP (Cambridge Serial Total Energy Package) package. The Perdew-Burke-Ernzerhof (PBE) functional within the framework of generalized gradient approximation (GGA) was applied to describe the electron-electron interactions. The van der Waals forces were considered based on a DFT-D3 correction method. For structural optimization, the Brillouin zone was sampled by 3×3×1 *k*-points for plane-wave basis, together with a energy cutoff of 750 eV. The convergence criterions were set to 0.01 eV/Å and 10^{-5} eV for Hellmann-Feymann force and total energy, respectively.

The formation Gibbs free energy (ΔG) of the NRR intermediates is calculated as [5]:

$$\Delta G = \Delta E + \Delta ZPE - T\Delta S + \Delta G_{\mathrm{U}} \tag{3}$$

where ΔE is the adsorption energy, ΔZPE is the zero point energy difference and $T\Delta S$ is the entropy difference between the gas phase and adsorbed state. $\Delta G_{\mathrm{U}} = -neU$, where n is the number of transferred charge and U is the electrode potential.

The adsorption energy (ΔE) was calculated by the following equation[5]

$$\Delta E = E_{\mathrm{ads/slab}} - E_{\mathrm{ads}} - E_{\mathrm{slab}} \tag{4}$$

where $E_{\mathrm{ads/slab}}$, E_{ads} and E_{slab} are the total energies for adsorbed species on slab, adsorbed species and isolated slab, respectively.

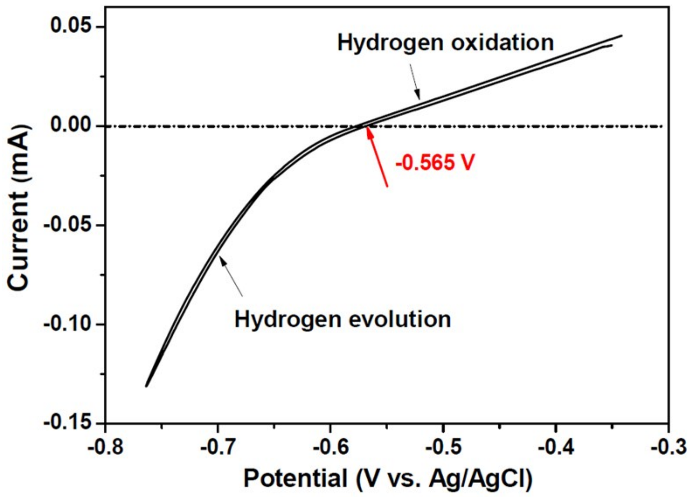

Fig. S1. The RHE calibration in 0.1 M Na_2SO_4 electrolyte.

The RHE calibration was carried out in the high-purity hydrogen saturated 0.1 M Na_2SO_4 electrolyte. The graphite rod and Pt wire were used as the counter and working electrodes, respectively. The cyclic voltammetry curves were performed at 1 mV s^{-1} scan rate. The RHE calibration potential for the hydrogen oxidation/evolution reactions is the average value of the two potentials at which the current crosses zero. Accordingly, it is shown in Fig. S1 that the E(RHE) is larger than E(Ag/AgCl) by 0.565 V, in good accordance with the value of 0.569 V calculated by the Nernst equation: $E_{\mathrm{RHE}} = E_{\mathrm{Ag/AgCl}} + 0.197 + 0.059 \times \mathrm{pH}$ (6.3).

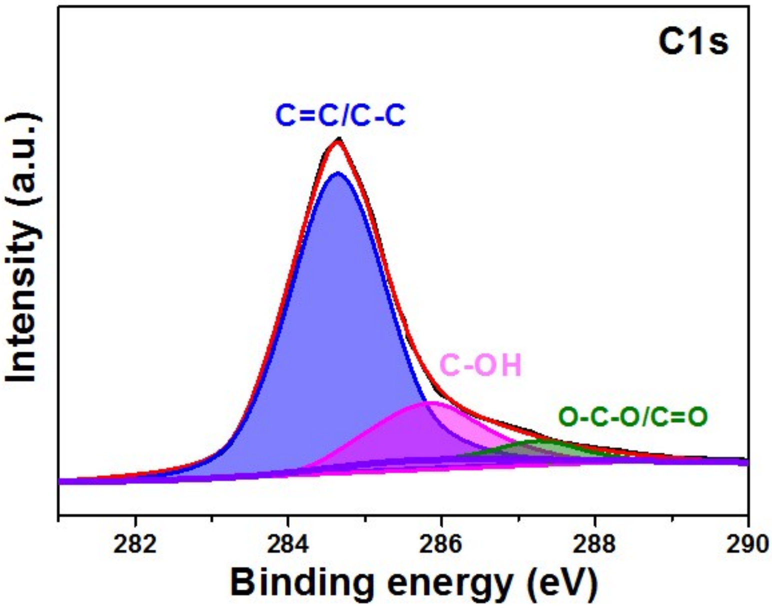

Fig. S2. XPS C1s spectra of MoO_2/RGO

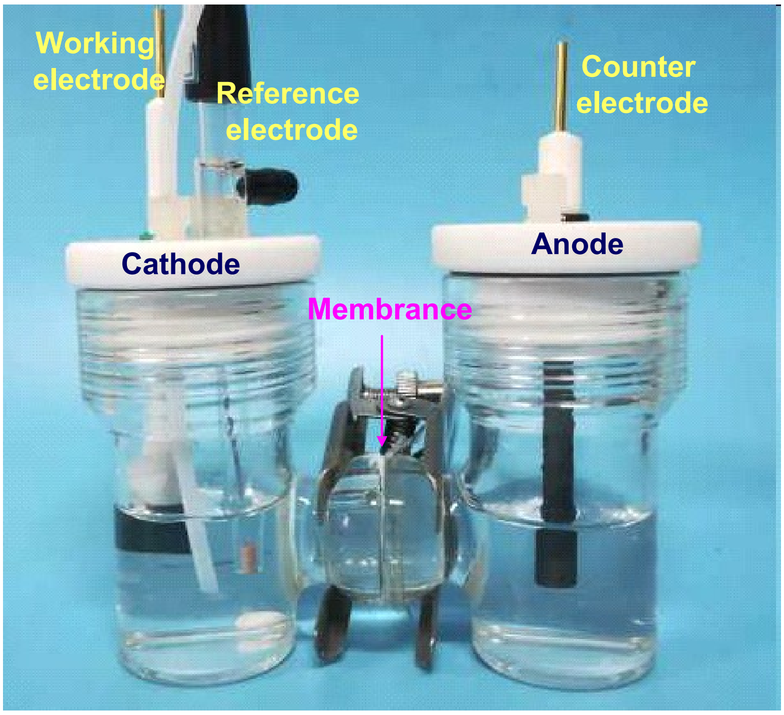

Fig. S3. Photograph of H-type electrochemical setup

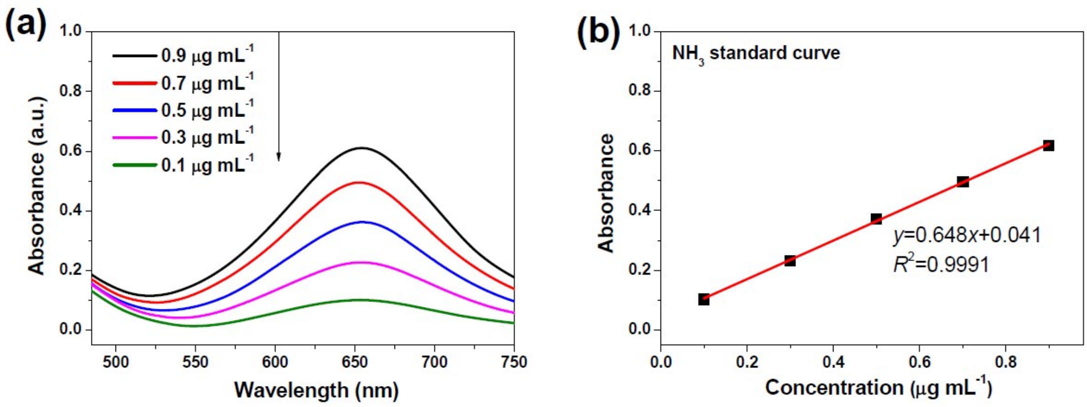

Fig. S4. (a) UV-Vis absorption spectra of indophenol assays with NH_4Cl in 0.1 M Na_2SO_4 after incubated for 2 h at ambient conditions. (b) Calibration curve used for calculation of NH_3 concentrations.

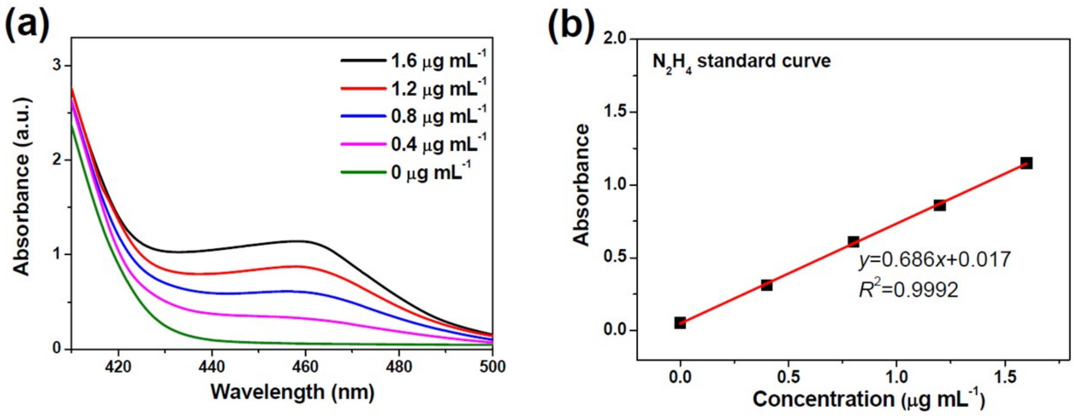

Fig. S5. (a) UV-Vis absorption spectra of N_2H_4 assays after incubated for 20 min at ambient conditions. (b) Calibration curve used for calculation of N_2H_4 concentrations.

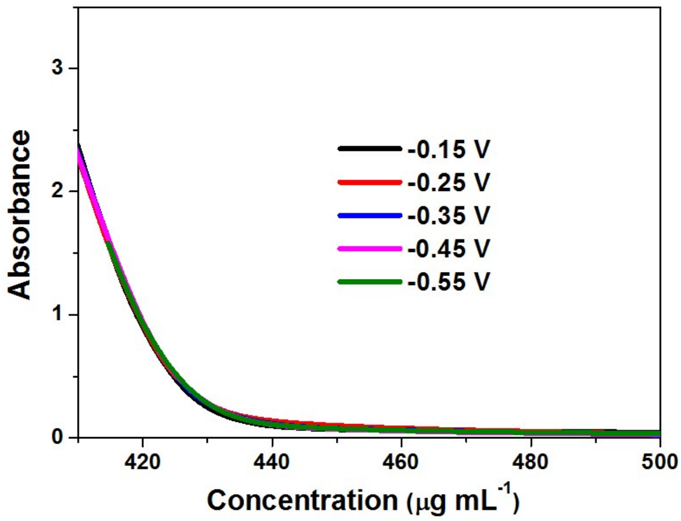

Fig. S6. UV-Vis spectra of the electrolytes (stained with the chemical indicator based on the method of Watt and Chrisp) after 2 h electrocatalysis on MoO_2/RGO at various potentials, and corresponding N_2H_4 concentrations in the electrolytes.

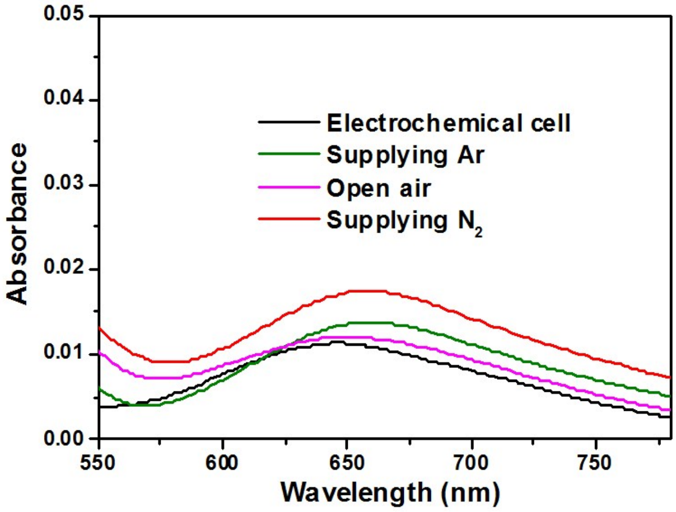

Fig. S7. UV-Vis absorption spectra of the electrolytes (stained with indophenol indicator) after standing for 2 h in open air of lab, or in electrochemical cell, or by continuously supplying N_2, as well continuously supplying Ar.

As reported in the literature[6], the NH_3 is ubiquitous in the laboratory environment and is a common contaminant in chemicals, especially gases, which may cause an overestimation of NRR performance. Therefore, before NRR electrolysis, the background NH_3 concentration in the laboratory environment was firstly conducted. As shown in Fig. S7, four cases of electrolytes, including standing for 2 h in open air of lab, or in electrochemical cell, or by continuously supplying N_2 gas, as well as continuously supplying Ar gas, show feeble signals of UV-Vis absorption spectra at a wavelength of ~650 nm, suggesting the existence of trace amount of NH_3 in the laboratory environment. The background NH_3 concentration can thus be determined to be in the range of 0.023~0.015 μg mL^{-1} with the average of 0.019 μg mL^{-1}.

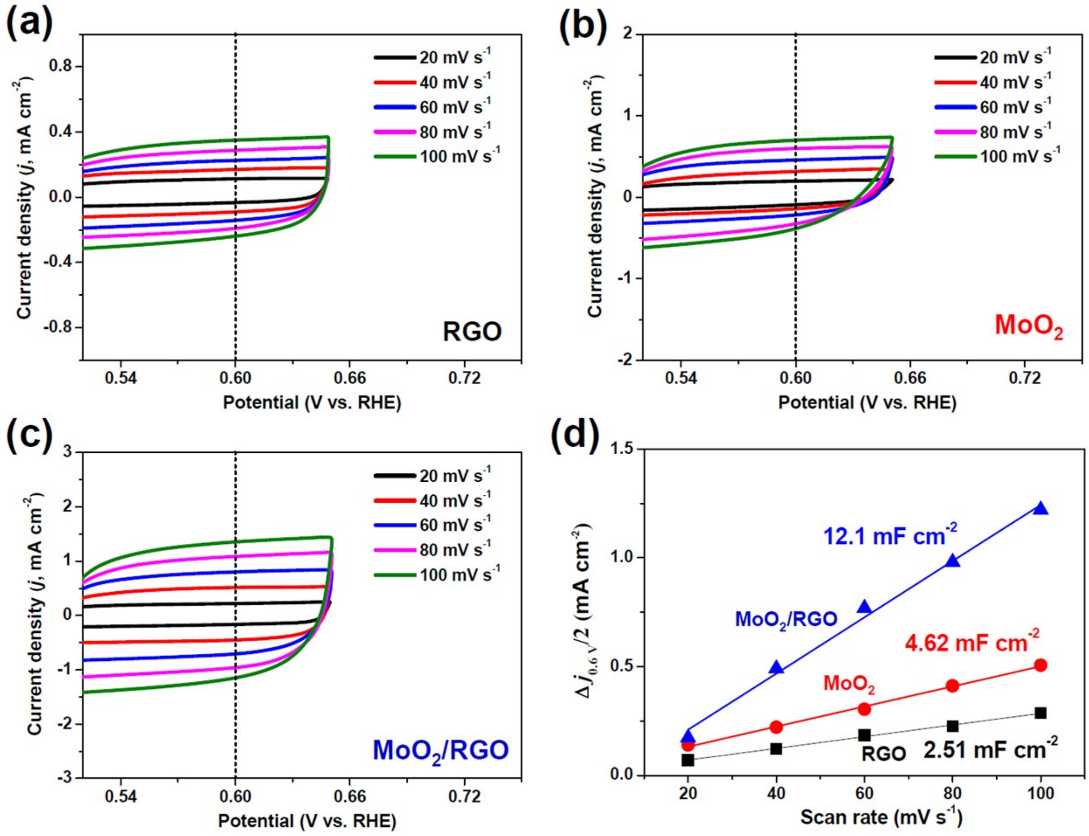

Fig. S8. (a-c) Cyclic voltammograms (CVs) of RGO, MoO_2 and MoO_2/RGO at different scan rates, and (d) corresponding determinations of electrochemical double-layer capacitance (C_{dl}).

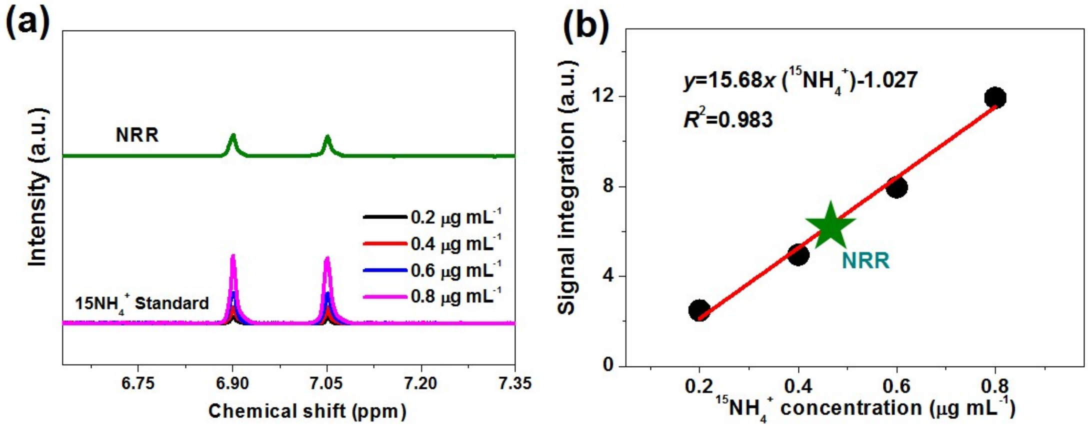

Fig. S9. (a) ^{1}H NMR spectra of $^{15}NH_4^+$ standard samples with different concentrations, as well as the ^{1}H NMR spectra of the electrolyte after NRR electrolysis on MoO_2/RGO for 2 h at -0.35 V. (b) The corresponding calibration curve of $^{15}NH_4^+$ concentration vs. peak area for $^{15}NH_4^+$ standard samples, together with the determined $^{15}NH_4^+$ concentrations of the electrolyte after NRR.

It is well accepted that the peak area of NMR spectra can be intimately related to the NH_3 concentration[7, 8], and thus the NH_3 concentration can be quantitatively determined by the NMR test. As shown in Fig. S9b, the calibration curve presents that the estimated peak areas of standard samples are linearly proportional to $^{15}NH_4^+$ concentrations. According to the calibration curve, the electrolyte after NRR for 2 h at -0.35 V presents the $^{15}NH_4^+$ concentration of 0.431 μg mL^{-1}, which agrees well with 0.458 μg mL^{-1} obtained by the indophenol blue method within the reasonable margin of experimental error.

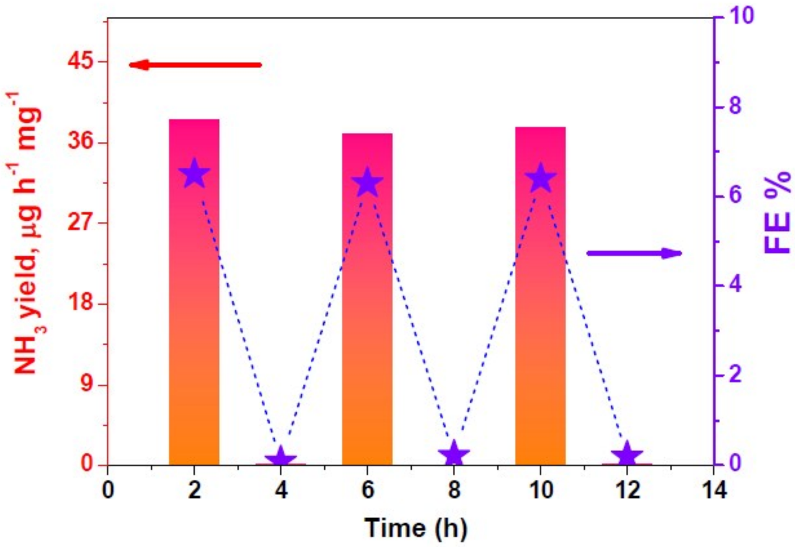

Fig. S10. Alternating cycling test of MoO_2/RGO by switching electrolysis between Ar-saturated and N_2-saturated solutions for 12 h at −0.35 V.

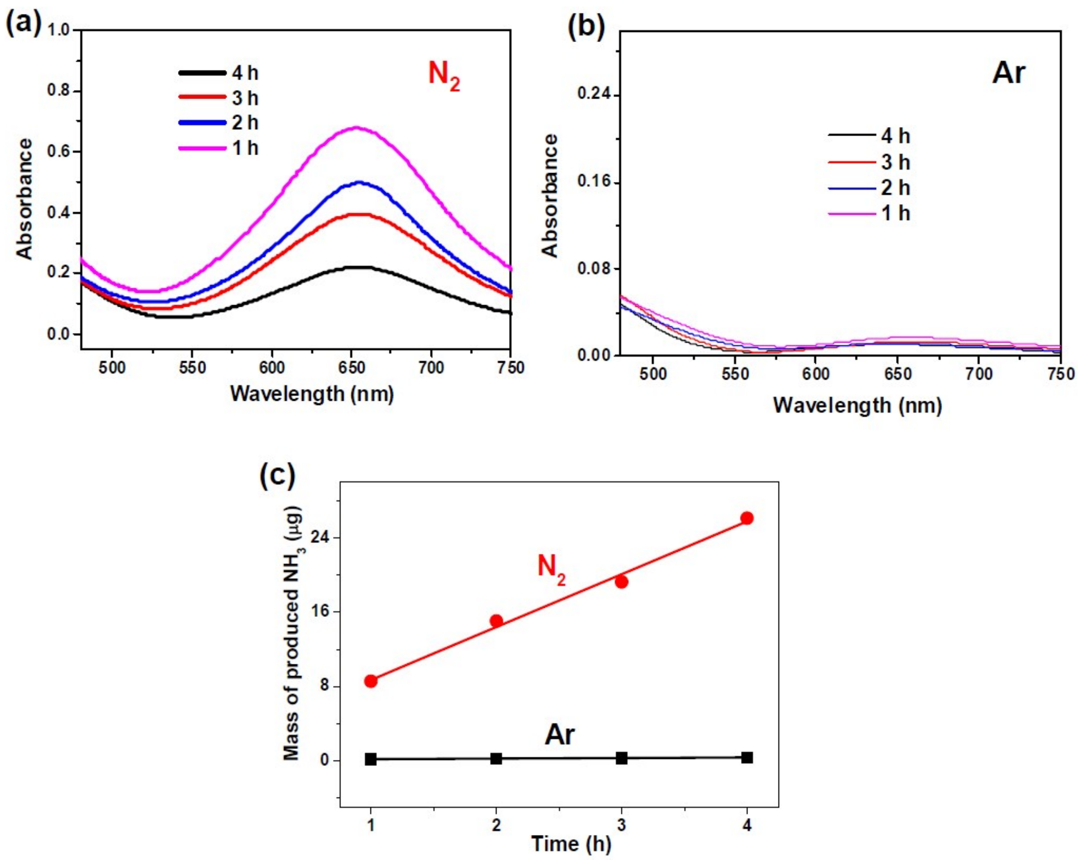

Fig. S11. (a, b) UV-Vis absorption spectra of the electrolytes stained with indophenol indicator after electrolysis in (a) N_2-saturated and (b) Ar-saturated solution at various times on MoO_2/RGO at -0.35 V, and (c) corresponding mass of produced NH_3.

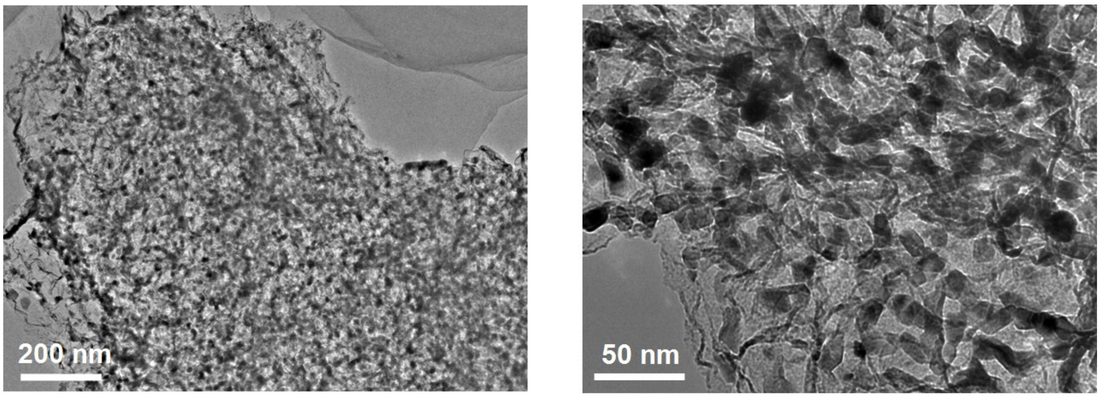

Fig. S12. TEM images of MoO_2/RGO after stability test.

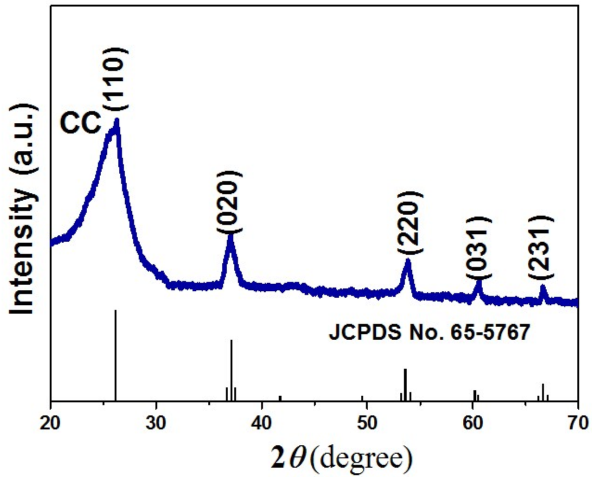

Fig. S13. XRD pattern of MoO_2/RGO after stability test.

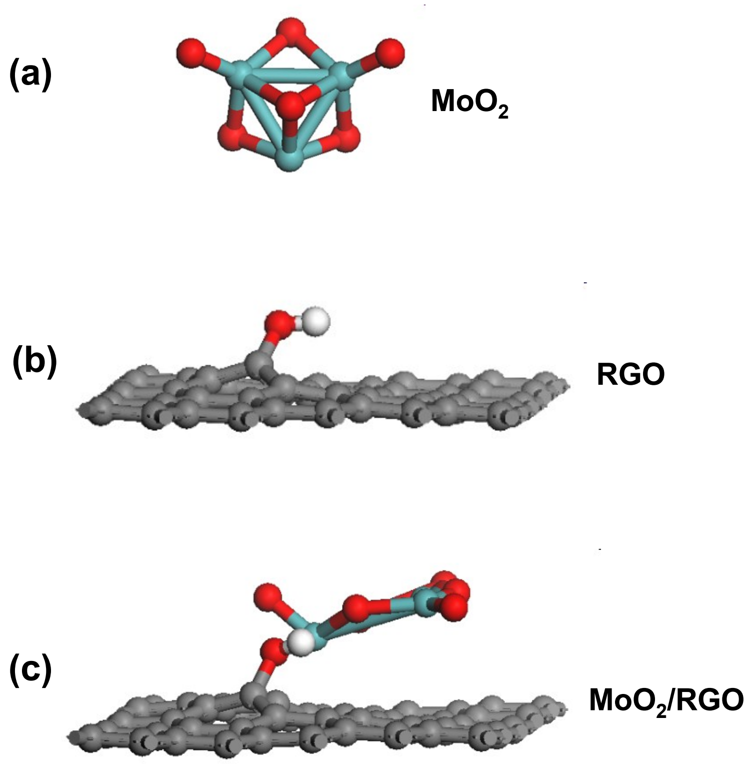

Fig. S14. Optimized structures of (a) MoO_2, (b) RGO and (c) MoO_2/RGO. Dark green, red, black and white spheres represent Mo, O, C and H atoms, respectively.

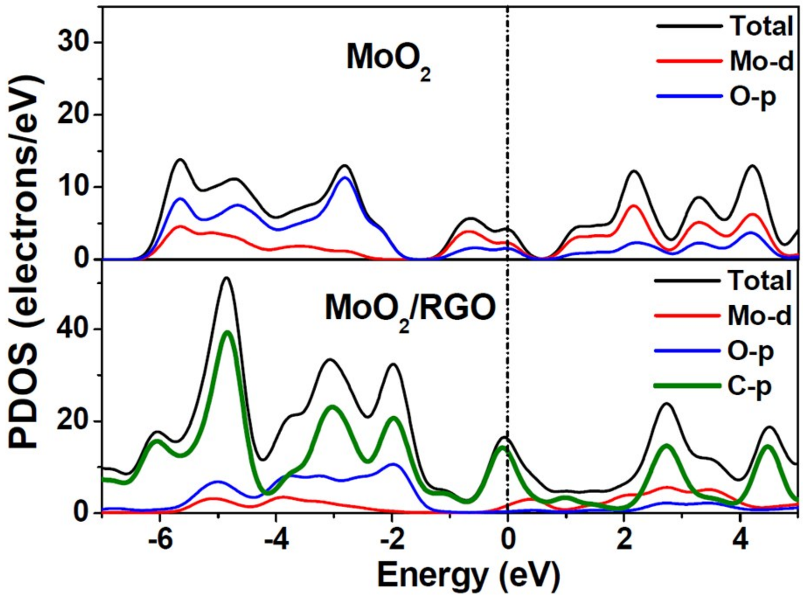

Fig. S15. Projected density of states (PDOS) of MoO_2 and MoO_2/RGO.

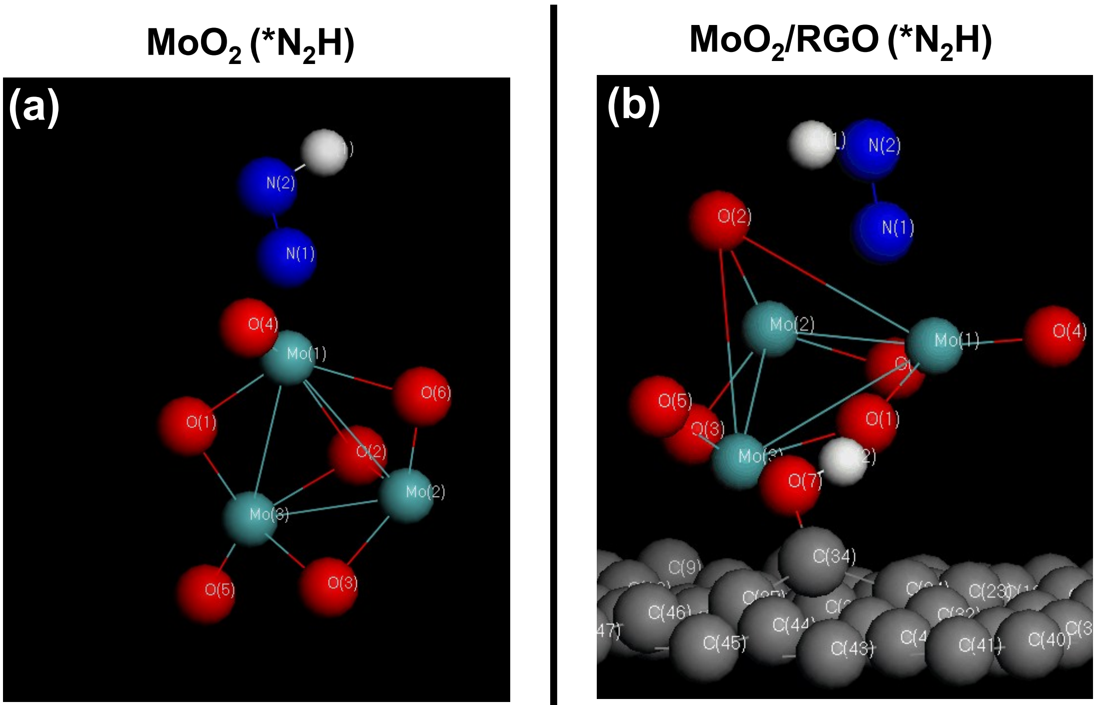

Atom	Charge (e)
Mo(1)	1.45
Mo(2)	0.98
Mo(3)	1.46
N(1)	-0.22
N(2)	-0.41

Atom	Charge (e)
Mo(1)	1.54
Mo(2)	1.22
Mo(3)	1.81
N(1)	-0.29
N(2)	-0.45

Fig. S16. Mulliken charge analysis of MoO_2 and MoO_2/RGO after binding *N_2H.

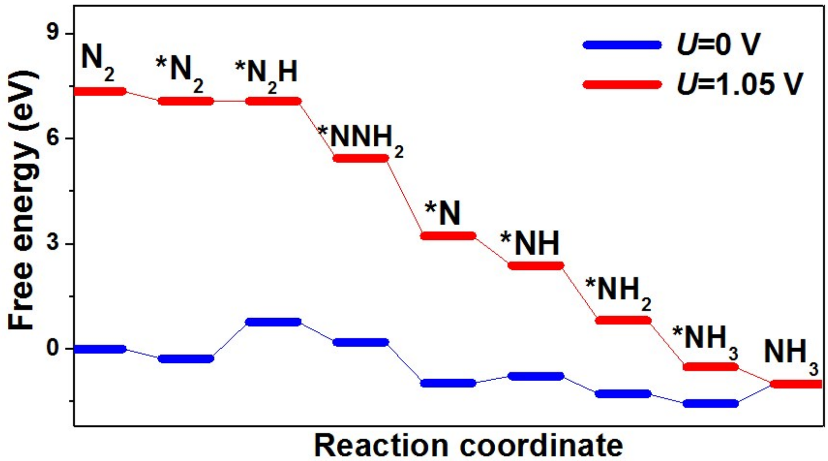

Fig. S17. Free energy diagrams of distal NRR pathway on MoO_2/RGO at zero and external applied energy (*U*) of -1.05 V.

Table S1. Comparison of NH_3 yield and Faradic efficiency (FE) for MoO_2/RGO with recently reported NRR electrocatalysts at ambient conditions

Catalyst	Electrolyte	Potential (V vs RHE)	NH_3 yield rate	FE (%)	Ref.
MoO_2/RGO	0.1 M Na_2SO_4	-0.35	37.4 $\mu g\ h^{-1}\ mg^{-1}$	6.6	This work
Mo nanofilm	H_2O	-0.49	1.89 $\mu g\ cm^{-2}\ h^{-1}$	0.72	[9]
Fe_2O_3-CNT	0.5 M KOH	-2	0.649 $\mu g\ cm^{-2}\ h^{-1}$	0.164	[10]
Rh nanosheets	0.1 M KOH	-0.2	23.88 $\mu g\ h^{-1}\ mg^{-1}$	0.217	[11]
Pd/C	0.1 M PBS	0.1	4.5 $\mu g\ h^{-1}\ mg^{-1}$	8.2	[12]
$Bi_4V_2O_{11}$-CeO_2 nanofibers	0.1 M HCl	-0.2	23.21 $\mu g\ h^{-1}\ mg^{-1}$	10.16	[13]
CoP hollow nanocage	1.0 M KOH	-0.4	10.78 $\mu g\ h^{-1}\ mg^{-1}$	7.36	[14]
$VN_{0.7}O_{0.45}$	Nafion	-0.1	3.31×10^{-10} mol s^{-1} cm^{-2}	5.95	[15]
MoO_2 with oxygen vacancies	0.1 M HCl	-0.15	12.2 $\mu g\ h^{-1}\ mg^{-1}$	8.2	[16]
Mosaic Bi nanosheets	0.1 M Na_2SO_4	-0.8	13.23 $\mu g\ h^{-1}\ mg^{-1}$	10.46	[17]
Ru single atoms/NPC	0.05 M H_2SO_4	-0.2	120.9 $\mu g\ h^{-1}\ mg^{-1}$	29.6	[18]
Mo_2C/C	0.5 M Li_2SO_4	-0.3	11.3 $\mu g\ h^{-1}\ mg^{-1}$	7.8	[7]
MXene	0.5 M Li_2SO_4	-0.1	4.7 $\mu g\ cm^{-2}\ h^{-1}$	5.78	[19]
Ru single-atoms/Zn	0.1 M HCl	-0.17	3.665 $\mu g\ h^{-1}\ mg^{-1}$	21	[20]
Black Phosphorus	0.01 M HCl	-0.6	31.37 $\mu g\ h^{-1}\ mg^{-1}$	5.07	[8]
Au nanorods	0.1 M KOH	-0.2	1.65 $\mu g\ cm^{-2}\ h^{-1}$	4.02	[21]
Amorphous $Pd_{0.2}Cu_{0.8}$/RGO	0.1 M KOH	-0.2	2.8 $\mu g\ h^{-1}\ mg^{-1}$	0.6	[22]
$BiVO_4$ with oxygen vacancies	0.2 M Na_2SO_4	-0.5	8.6 $\mu g\ h^{-1}\ mg^{-1}$	10.4	[23]
MoS_2 with Li-S Interactions	0.1 M Li_2SO_4	-0.2	43.4 $\mu g\ h^{-1}\ mg^{-1}$	9.81	[24]
B_4C nanosheet	0.1 M HCl	-0.75	26.57 $\mu g\ h^{-1}\ mg^{-1}$	15.95	[25]
MoS_2 nanosheet	0.1 M Na_2SO_4	-0.5	8.08×10^{-11} mol s^{-1} cm^{-2}	1.17	[4]
MoO_3 nanosheets	0.1 M HCl	-0.5	4.80×10^{-10} mol s^{-1} cm^{-2}	1.9	[26]
Mo_2N nanorods	0.1 M HCl	-0.3	78.4 $\mu g\ h^{-1}\ mg^{-1}$	4.5	[27]

MoN nanosheets	0.1 M HCl	-0.3	3.01×10^{-10} mol s^{-1} cm^{-2}	1.15	[28]
Mo_2C nanorod	0.1 M HCl	-0.3	95.1 μg h^{-1} mg^{-1}	8.13	[29]
MoS_2/RGO	0.1 M HCl	-0.45	24.82 μg h^{-1} mg^{-1}	4.58	[30]
Cr_2O_3/RGO	0.1 M HCl	-0.6	33.3 μg h^{-1} mg^{-1}	7.33	[31]
B-doped graphene	0.05 M H_2SO_4	-0.5	9.8 μg cm^{-2} h^{-1}	10.8	[32]
N-doped porous carbon	0.05 M H_2SO_4	-0.9	1.4 mmol g^{-1} h^{-1}	1.42	[33]

Supplementary references

[1] Q. Tang, Z. Shan, L. Wang and X. Qin, *Electrochim. Acta*, 2012, **79**, 148-153.
[2] D. Zhu, L. Zhang, R. E. Ruther and R. J. Hamers, *Nat. Mater.*, 2013, **12**, 836.
[3] G. W. Watt and J. D. Chrisp, *Anal. Chem.*, 1952, **24**, 2006-2008.
[4] L. Zhang, X. Ji, X. Ren, Y. Ma, X. Shi, Z. Tian, A. M. Asiri, L. Chen, B. Tang and X. Sun, *Adv. Mater.*, 2018, **30**, 1800191.
[5] A. A. Peterson, *Energy Environ. Sci.*, 2010, **3**, 1311-1315.
[6] B. H. R. Suryanto, H.-L. Du, D. Wang, J. Chen, A. N. Simonov and D. R. MacFarlane, *Nat. Catal.*, 2019, **2**, 290-296.
[7] H. Cheng, L. X. Ding, G. F. Chen, L. Zhang, J. Xue and H. Wang, *Adv. Mater.*, 2018, **30**, 1803694.
[8] L. L. Zhang, L. X. Ding, G. F. Chen, X. F. Yang and H. H. Wang, *Angew. Chem. Int. Edit.*, 2019, **131**, 2638-2642.
[9] D. Yang, T. Chen and Z. Wang, *J. Mater. Chem. A*, 2017, **5**, 18967-18971.
[10] S. Chen, S. Perathoner, C. Ampelli, C. Mebrahtu, D. Su and G. Centi, *Angew. Chem. Int. Edit.*, 2017, **56**, 2699-2703.
[11] H. M. Liu, S. H. Han, Y. Zhao, Y. Y. Zhu, X. L. Tian, J. H. Zeng, J. X. Jiang, B. Y. Xia and Y. Chen, *J. Mater. Chem. A*, 2018, **6**, 3211-3217.
[12] J. Wang, L. Yu, L. Hu, G. Chen, H. Xin and X. Feng, *Nat. Commun.*, 2018, **9**, 1795.
[13] C. Lv, C. Yan, G. Chen, Y. Ding, J. Sun, Y. Zhou and G. Yu, *Angew. Chem. Int. Edit.*, 2018, **130**, 6181-6184.
[14] W. Guo, Z. Liang, J. Zhao, B. Zhu, K. Cai, R. Zou and Q. Xu, *Small Methods*, 2018, 1800204.
[15] X. Yang, J. Nash, J. Anibal, M. Dunwell, S. Kattel, E. Stavitski, K. Attenkofer, J. G. Chen, Y. Yan and B. Xu, *J. Am. Chem. Soc.*, 2018, 13387-13391.
[16] G. Zhang, Q. Ji, K. Zhang, Y. Chen, Z. Li, H. Liu, J. Li and J. Qu, *Nano Energy*, 2019, **59**, 10-16.
[17] L. Li, C. Tang, B. Xia, H. Jin, Y. Zheng and S.-Z. Qiao, *ACS Catal.*, 2019, **9**, 2902-2908.
[18] Z. Geng, Y. Liu, X. Kong, P. Li, K. Li, Z. Liu, J. Du, M. Shu, R. Si and J. Zeng, *Adv. Mater.*, 2018, **30**, 1803498.
[19] Y. R. Luo, G. F. Chen, L. Ding, X. Z. Chen, L. X. Ding and H. H. Wang, *Joule*, 2019, **3**, 279-289.
[20] H. Tao, C. Choi, L.-X. Ding, Z. Jiang, Z. Han, M. Jia, Q. Fan, Y. Gao, H. Wang and A. W. Robertson, *Chem*, 2018, **5**, 204-214.
[21] D. Bao, Q. Zhang, F. L. Meng, H. X. Zhong, M. M. Shi, Y. Zhang, J. M. Yan, Q. Jiang and X. B. Zhang, *Adv. Mater.*, 2017, **29**, 1604799.
[22] M. M. Shi, D. Bao, S. J. Li, B. R. Wulan, J. M. Yan and Q. Jiang, *Adv. Energy. Mater.*, 2018, **8**, 1800124.
[23] J. X. Yao, D. Bao, Q. Zhang, M. M. Shi, Y. Wang, R. Gao, J. M. Yan and Q. Jiang, *Small Methods*, 2018, 1800333.
[24] Y. Liu, M. Han, Q. Xiong, S. Zhang, C. Zhao, W. Gong, G. Wang, H. Zhang and H. Zhao, *Adv. Energy. Mater.*, 2019, **9**, 1803935.
[25] W. Qiu, X.-Y. Xie, J. Qiu, W.-H. Fang, R. Liang, X. Ren, X. Ji, G. Cui, A. M. Asiri and G. Cui, *Nat. Commun.*, 2018, **9**, 3485.
[26] J. Han, X. Ji, X. Ren, G. Cui, L. Li, F. Xie, H. Wang, B. Li and X. Sun, *J. Mater. Chem. A*, 2018, **6**, 12974-12977.
[27] X. Ren, G. Cui, L. Chen, F. Xie, Q. Wei, Z. Tian and X. Sun, *Chem. Commun.*, 2018, **54**, 8474-8477.
[28] L. Zhang, X. Ji, X. Ren, Y. Luo, X. Shi, A. M. Asiri, B. Zheng and X. Sun, *ACS Sustain. Chem. Eng.*, 2018,

6, 9550-9554.
[29] X. Ren, J. Zhao, Q. Wei, Y. Ma, H. Guo, Q. Liu, Y. Wang, G. Cui, A. M. Asiri, B. Li, B. Tang and X. Sun, *ACS Central Sci.*, 2019, **5**, 116-121.
[30] X. Li, X. Ren, X. Liu, J. Zhao, X. Sun, Y. Zhang, X. Kuang, T. Yan, Q. Wei and D. Wu, *J. Mater. Chem. A*, 2019, **7**, 2524-2528.
[31] L. Xia, B. Li, Y. Zhang, R. Zhang, L. Ji, H. Chen, G. Cui, H. Zheng, X. Sun, F. Xie and Q. Liu, *Inorg. Chem.*, 2019, **58**, 2257-2260.
[32] X. Yu, P. Han, Z. Wei, L. Huang, Z. Gu, S. Peng, J. Ma and G. Zheng, *Joule*, 2018, **2**, 1610-1622.
[33] Y. Liu, Y. Su, X. Quan, X. Fan, S. Chen, H. Yu, H. Zhao, Y. Zhang and J. Zhao, *ACS Catal.*, 2018, **8**, 1186-1191.